Testing the Isotropy of the Dark Energy Survey's Extreme Trans-Neptunian Objects

Pedro H. Bernardinelli[1] , Gary M. Bernstein[1] , Masao Sako[1] , Stephanie Hamilton[2] , David W. Gerdes[2,3] ,
Fred C. Adams[2,3] , William R. Saunders[1,4] , M. Aguena[5,6], S. Allam[7], S. Avila[8], D. Brooks[9], H. T. Diehl[7], P. Doel[9], S. Everett[10],
J. García-Bellido[8], E. Gaztanaga[11,12] , R. A. Gruendl[13,14] , K. Honscheid[15,16], R. L. C. Ogando[6,17], A. Palmese[7,18] ,
D. L. Tucker[7], A. R. Walker[19] , and W. Wester[7]
(The DES Collaboration)

[1] Department of Physics and Astronomy, University of Pennsylvania, Philadelphia, PA 19104, USA; pedrobe@sas.upenn.edu
[2] Department of Physics, University of Michigan, Ann Arbor, MI 48109, USA; sjhamil@umich.edu
[3] Department of Astronomy, University of Michigan, Ann Arbor, MI 48109, USA
[4] Department of Astronomy, Boston University, Boston, MA 02215, USA
[5] Departamento de Física Matemática, Instituto de Física, Universidade de São Paulo, CP 66318, São Paulo, SP, 05314-970, Brazil
[6] Laboratório Interinstitucional de e-Astronomia—LIneA, Rua Gal. José Cristino 77, Rio de Janeiro, RJ—20921-400, Brazil
[7] Fermi National Accelerator Laboratory, P.O. Box 500, Batavia, IL 60510, USA
[8] Instituto de Fisica Teorica UAM/CSIC, Universidad Autonoma de Madrid, E-28049 Madrid, Spain
[9] Department of Physics & Astronomy, University College London, Gower Street, London, WC1E 6BT, UK
[10] Santa Cruz Institute for Particle Physics, Santa Cruz, CA 95064, USA
[11] Institut d'Estudis Espacials de Catalunya (IEEC), E-08034 Barcelona, Spain
[12] Institute of Space Sciences (ICE, CSIC), Campus UAB, Carrer de Can Magrans, s/n, E-08193 Barcelona, Spain
[13] Department of Astronomy, University of Illinois at Urbana-Champaign, 1002 W. Green Street, Urbana, IL 61801, USA
[14] National Center for Supercomputing Applications, 1205 West Clark St., Urbana, IL 61801, USA
[15] Center for Cosmology and Astro-Particle Physics, The Ohio State University, Columbus, OH 43210, USA
[16] Department of Physics, The Ohio State University, Columbus, OH 43210, USA
[17] Observatório Nacional, Rua Gal. José Cristino 77, Rio de Janeiro, RJ—20921-400, Brazil
[18] Kavli Institute for Cosmological Physics, University of Chicago, Chicago, IL 60637, USA
[19] Cerro Tololo Inter-American Observatory, NSF's National Optical-Infrared Astronomy Research Laboratory, Casilla 603, La Serena, Chile

Abstract

We test whether the population of "extreme" trans-Neptunian objects (eTNOs) detected in the first four years of the Dark Energy Survey (DES Y4) data exhibit azimuthal asymmetries that might be evidence of gravitational perturbations from an unseen super-Earth in a distant orbit. By rotating the orbits of the detected eTNOs, we construct a synthetic population that, when subject to the DES selection function, reproduces the detected distribution of eTNOs in the orbital elements a, e, and i as well as absolute magnitude H, but has uniform distributions in mean anomaly $\mathcal{M}$, longitude of ascending node Ω, and argument of perihelion ω. We then compare the detected distributions in each of Ω, ω, and the longitude of perihelion $\varpi \equiv \Omega + \omega$ to those expected from the isotropic population, using Kuiper's variant of the Kolmogorov–Smirnov test. The three angles are tested for each of four definitions of the eTNO population, choosing among $a > (150, 250)$ au and perihelion $q > (30, 37)$ au. These choices yield 3–7 eTNOs in the DES Y4 sample. Among the 12 total tests, two have the likelihood of drawing the observed angles from the isotropic population at $p < 0.03$. The three detections at $a > 250$ and $q > 37$ au and the four detections at $a > 250$ and $q > 30$ au have a Ω distribution with $p \approx 0.03$ coming from the isotropic construction, but this is not strong evidence of anisotropy given the 12 different tests. The DES data taken on their own are thus consistent with azimuthal isotropy and do not require a "Planet 9" hypothesis. The limited sky coverage and object count mean, however, that the DES data by no means falsify this hypothesis.

Unified Astronomy Thesaurus concepts: Trans-Neptunian objects (1705); Kuiper belt (893)

1. Introduction

Trujillo & Sheppard (2014) noted that the sample of then-known trans-Neptunian objects (TNOs) with a semimajor axis of $a > 150$ au and a perihelion of $q > 30$ au seemed clustered in their arguments of perihelion near $\omega \approx 0°$. Batygin & Brown (2016a) argue that TNOs with $a > 250$ au are also clustered in their longitude of ascending node at $90° \lesssim \Omega \lesssim 180°$, defining the direction of the orbital pole. They also find clustering in the longitude of perihelion at $0° \lesssim \varpi \equiv \Omega + \omega \lesssim 90°$ (the apsidal

orientation of the orbit), which would indicate a physical alignment of the orbits. The hypothesized dynamical mechanism to stabilize these angles is the presence of a distant planetary-mass perturber ("Planet 9"), which was extensively reviewed in Batygin et al. (2019), but the question remains as to the statistical significance of this clustering in the face of survey selection effects (Lawler et al. 2017; Shankman et al. 2017; Kavelaars et al. 2020). The proposed perturber can also generate high-inclination orbits (Batygin & Brown 2016b; Batygin & Morbidelli 2017) and in some scenarios can account for the obliquity of the Sun (Bailey et al. 2016; Lai 2016; Gomes et al. 2017). The inclination instability mechanism proposed in Madigan & McCourt (2016) can also potentially account for both the argument of perihelion and apsidal clustering (Zderic et al. 2020) without a ninth planet.

Since Trujillo & Sheppard (2014), numerous other of these "extreme" TNOs (eTNOs, $a > 150$ au and $q > 30$ au) have been discovered (Bannister et al. 2016, 2018; Sheppard & Trujillo 2016; Becker et al. 2018; Khain et al. 2018, 2020; Sheppard et al. 2019; Bernardinelli et al. 2020). Shankman et al. (2017) present an analysis of the Outer Solar System Origins Survey (OSSOS; Bannister et al. 2016, 2018) sample of eTNOs, using a survey simulator to demonstrate the nonintuitive biases involved in detecting such objects and to conclude that the distribution of the eight OSSOS eTNOs is consistent with uniformity in Ω, ω, and ϖ.[20] Sheppard et al. (2019) find a modest-significance clustering in the objects with low observational biases, and the analysis of the Minor Planet Center sample by Batygin & Brown (2016a), Brown (2017), and Brown & Batygin (2019) find that there is a small chance of accidental clustering of these objects, albeit with less complete information about the selection function of the discovery surveys. Trujillo (2020) reviews the observational evidence and the statistical significance of the alignment in the distant TNO populations.

We conduct here an independent test of azimuthal isotropy using the eTNOs detected by the Dark Energy Survey (DES; Bernardinelli et al. 2020), fully accounting for this survey's observational characteristics and recoverability. More precisely, we seek a model of the underlying population of eTNOs that (1) is uniformly distributed in Ω and ω (and hence in ϖ) as well as in mean anomaly $\mathcal{M}$ and that (2) after applying the survey selection function, predicts a distribution in $\{a, e, i, H, \Omega, \omega\}$ that is consistent with that of the true eTNO sample. If we find such an isotropic distribution that matches the observations, we cannot claim evidence of orbital alignments in the first four years (Y4) of the DES eTNO sample. A similar analysis using this survey's difference-imaging sample has been presented in Hamilton (2019) and is summarized in Section 5.

2. Sample of eTNOs

The DES surveyed 5000 deg^2 of sky repeatedly over six observing seasons (2013–2019) with the 3 deg^2 520 Mpix Dark Energy Camera (DECam; Flaugher et al. 2015) in the $grizY$ optical/near-infrared (NIR) bands. The full (wide) survey tiles the footprint with 10×90 s exposures in the $griz$ bands and $6 \times 45 + 2 \times 90$ s exposures in the Y band, with a total of $\approx 80{,}000$ exposures. Bernardinelli et al. (2020) describe the methodology that allows the recovery of TNOs in the DES and present a catalog of 316 TNOs detected in the first four years of the survey (Y4, $\approx 60{,}000$ images), with typical r-band exposures being complete to $r \sim 23.5$. These objects have multi-year arcs, at least six unique nights of detections, and $grizY$ photometry, yielding uncertainties in orbital elements and H that are negligible for the isotropy test ($\frac{\sigma_a}{a} \lesssim 3\%$, $\sigma \lesssim 0°\!.5$ for all angular variables, and $\sigma_H \lesssim 0.1$ mag). Bernardinelli et al. (2020) also introduce a methodology for testing the completeness of the survey, which will be extended in this work.

Among the 316 objects of the Y4 sample, seven satisfy the original eTNO definition of Trujillo & Sheppard (2014): $a > 150$ au and $q > 30$ au. The barycentric orbital elements and absolute magnitudes of these objects are presented in Table 1. The ecliptic-plane projection of the orbits, as well as a projection of DES's footprint, are plotted in Figure 1. We refer

the reader to Figures 1 and 19 of Bernardinelli et al. (2020) for images of the full DES footprint. Given that the angular clustering in $\{\Omega, \omega, \varpi\}$ has been claimed to be present in a variety of subsets of this loosest definition, we will conduct our tests for four cases:

1. $a > 150$ au and $q > 30$ au (the full seven object set), as in Trujillo & Sheppard (2014);
2. $a > 250$ au and $q > 30$ au (four DES objects), where Batygin & Brown (2016a) find there is a clustering in Ω and ϖ;
3. $a > 150$ au and $q > 37$ au (four DES objects), eliminating objects with the stronger interactions with Neptune (Lykawka & Mukai 2007; also see a discussion in Shankman et al. 2017);
4. and $a > 250$ au and $q > 37$ au (three DES objects), combining both restrictions.

The objects belonging to the fourth case are the ones least influenced by Neptune and thus offer the cleanest test for influences from a Planet 9. Given the small observed population for case (4), however, the tests are going to be weak, and we are wise to also examine the less restrictive cases (1)–(3) despite potentially weaker signals.

We note that the DES eTNO sample has no overlap with the objects analyzed by Batygin & Brown (2016a), Brown (2017), and Sheppard et al. (2019), nor with the OSSOS sample of Shankman et al. (2017), thus making this test largely statistically independent of these predecessors. Despite this independence, the distributions of ω, Ω, and ϖ for the DES sample (see Table 1) show tendencies to lie in the ranges earlier suggested as being overpopulated. It is of interest, therefore, to see if the apparent clustering in this independent sample can be explained as a selection effect.

3. Simulated Isotropic Population

We use a simple construction to create a population that is isotropic in $\{\mathcal{M}, \Omega, \omega\}$ but predicts a distribution $p(a, e, i, H|s)$ (conditioned on successful detection s) that is consistent with that of the detected eTNOs. Indexing the latter by j, we posit an underlying population with

$$
\begin{aligned}
p(a, e, i, \Omega, \omega, \mathcal{M}, H) \propto \\
\sum_j \frac{\delta(a - a_j)\delta(e - e_j)\delta(i - i_j)\delta(H - H_j)}{p(s|a_j, e_j, i_j, H_j)} \\
\times\, u(\mathcal{M})u(\Omega)u(\omega).
\end{aligned} \quad (1)
$$

In this equation, $u(\theta)$ is a uniform distribution over $\theta \in [0, 2\pi]$, δ is the Dirac delta function, and $p(s|a, e, i, H)$ is the probability of detection of an eTNO in DES when averaged over $(\mathcal{M}, \Omega, \omega)$. In other words, we replicate each detected object, randomizing its Ω, ω, and $\mathcal{M}$, and weighting inversely by the fraction of randomized objects that are detected. It is then easy to see that the randomized ensemble has a distribution:

$$
\begin{aligned}
p(a, e, i, H|s) \propto \sum_j \delta(a - a_j)\delta(e - e_j) \\
\times\, \delta(i - i_j)\delta(H - H_j)
\end{aligned} \quad (2)
$$

and therefore is a precise match to the detected ensemble. While of course it is not a realistic model of the underlying

---

[20] Bannister et al. (2018) repeat the test with one more object.

Table 1
Barycentric Orbital Elements at Barycentric Julian Date 2016.0, Absolute r-band Magnitude, and r-band Magnitude at the Discovery for the Sample of eTNOs

MPC id	a (au)	e	i (deg)	Ω (deg)	ω (deg)	ϖ (deg)	q (au)	H_r	m_r	Cases
2013 RA$_{109}$	463.3(2)	0.901	12.39	104.79	262.91(1)	7.71	46.0	5.9	22.6	1,2,3,4,$\star$
2015 BP$_{519}$	449.3(8)	0.922	54.11	135.21	348.06	123.27	35.2(1)	4.3	21.7	1,2,$\star$
2013 SL$_{102}$	314.3(1)	0.879	6.50	94.73	265.49	0.22	38.1	7.1	22.9	1,2,3,4,$\star$
2014 WB$_{556}$	289.3(6.2)	0.853(3)	24.15	114.89	234.53(49)	−10.56	42.5(1.9)	7.2	23.7	1,2,3,4
2016 SG$_{58}$	233.0(1)	0.849	13.22	118.97	296.29	55.27	35.1	7.2	22.8	1
2016 QV$_{89}$	171.6(2)	0.767	21.38	173.21	281.08(1)	94.29	40.0(1)	5.9	22.8	1,3
508338 (2015 SO$_{20}$)	164.7	0.799	23.41	33.63	354.78(3)	28.42	33.2	6.6	21.8	1
2013 RF$_{98}$	358.2	0.90	23.54	67.63	312.05	19.68	36.1	8.6	24.2	$\star$

Note. See Bernardinelli et al. (2020) for more details and state vectors with full covariance matrices for these objects. The last column indicates which of the cases defined in Section 2 each object belongs to. Objects marked with "$\star$" were also used in the Hamilton (2019) analysis (Section 5). Uncertainties are given in parentheses when they exceed the printed precision (rigorous uncertainties are not available for 2013 RF$_{98}$, orbital elements obtained using JPL Horizons).

eTNO population, it is the simplest way to create a synthetic population that meets the criteria of isotropy and agreement with the distribution of "uninteresting" parameters.

To realize the simulated population described by Equation (1), we start by creating 40 million clones of each detected eTNO j for which Ω, ω, and $\mathcal{M}$ have been redistributed uniformly while retaining a, e, i, and H. We limit the sampling of $\mathcal{M}$ to be uniform between $-15°$ and $15°$, as all of the detected objects would be too distant and faint to be detected outside this range. This limited sampling translates to a normalization factor of $30/360$ in each $p(s|a_j, e_j, i_j, H_j)$. Since we are only interested in relative detection probabilities, this normalization can be safely ignored.

For each member of the simulated swarm, we determine all exposures for which the object would be inside a functional DECam CCD and proceed to use the probability $p(m)$ that a point source with magnitude m would be detected in this exposure (see Section 2.6 of Bernardinelli et al. 2020). If $p(m)$ for the simulated object's m is larger than a random unit deviate, this observation is considered a detection of this object.

Once we evaluate all exposures that contain the orbit, we apply the selection criteria used by Bernardinelli et al. (2020) for the DES Y4 search: the number of unique nights in which an object was detected must satisfy NUNIQUE $\geqslant 6$, the length of the orbital arc must satisfy ARC > 6 months, and the shortest arc that remains after eliminating any one night of detections must also satisfy ARCCUT > 6 months.

The fraction of all simulated clones of object j that survive these cuts defines the $p(s|a, e, i, H)$ that is in the denominator of Equation (1). Once the simulation is complete, we can calculate the expected $p(\Omega|s)$, $p(\omega|s)$ and $p(\varpi|s)$ of the isotropic population by a histogram of the values for all the clones deemed as detections, weighting inversely by the $p(s)$ values. Normalizing the histograms to unit integral yields estimates of the probability of detection of an eTNO with angle $\theta \in \{\omega, \Omega, \varpi\}$. If an object satisfies more than one of our four cases of eTNO definitions, we reuse a single set of clones for all cases, leading to correlations in the small-scale noise of the probabilities for different cases.

Figure 2 shows these angular selection functions for each of the four eTNO definitions and each of the three angles. We note to begin that the selection functions are very similar for all four cases, suggesting that these functions are robust to details of the definition of the $\{a, e, i, H\}$ distribution. The DES selection function for the longitude of perihelion (ϖ) is seen to be quite narrow. This is not surprising, since the DES footprint

is confined to a narrow range of ecliptic longitude, and we will have a strong bias toward objects that reach perihelion within the footprint, particularly for the high e's typical of eTNOs. The strong bias in Ω seen in Figure 2 is also easily understood as a consequence of the DES footprint being almost entirely in the southern ecliptic hemisphere in a limited range of ecliptic longitude.

4. Isotropy Tests

We compare the $p(\theta|s)$ probability distributions derived for an underlying azimuthally isotropic population to the observed distribution of $\theta \in \{\Omega, \omega, \varpi\}$ by applying Kuiper's test (Kuiper 1960), which is an extension of the Kolmogorov–Smirnov test that is invariant under cyclic permutations as well as being sensitive both in the median and in the tails of the distribution. For each case of eTNO definition, the significance of this test is measured by computing Kuiper's statistic V_{real} for the true detected eTNOs to the V_{fake} values computed for 10^6 sets of simulated detections sampled from the isotropized distribution. The p-value is the fraction of times $V_{\text{fake}} > V_{\text{real}}$, i.e., the probability that a Kuiper statistic value as high as the one observed would arise if the angles were drawn from the isotropic population. A test with a p-value of 0.05 rejects the null hypothesis with 95% confidence, with lower p-values increasing this confidence. We note that this isotropy test is similar to Shankman et al. (2017)'s test on the OSSOS data, in which a population model for eTNOs is built for the null hypothesis. Table 2 reports the p-value of this test for each combination of orbital angle and eTNO definition for a total of 12 tests.

The p-values for the Kuiper test indicate that the DES observations are consistent with being drawn from the isotropic population model, with the possible exception of a low-significance discrepancy ($p \approx 0.025$) in the longitude of ascending node (Ω) distribution for cases (2) and (4) at $a > 250$ au. Note that we have performed 12 distinct tests in a small data set, so we cannot claim a significant clustering from a single test at this p-value. Given that the 12 tests are highly correlated, we unfortunately have no straightforward means of determining an overall significance of the ensemble. If the tests were fully correlated, then of course the chances of observing one at $p \leqslant 0.024$ in an isotropic population would be 2.4%. If the 12 tests were fully uncorrelated, the chance of having $p \leqslant 0.024$ in one or more tests would be $1 - (0.976)^{12} = 25\%$; these can be considered lower and upper bounds on the overall significance of anisotropy. The p-
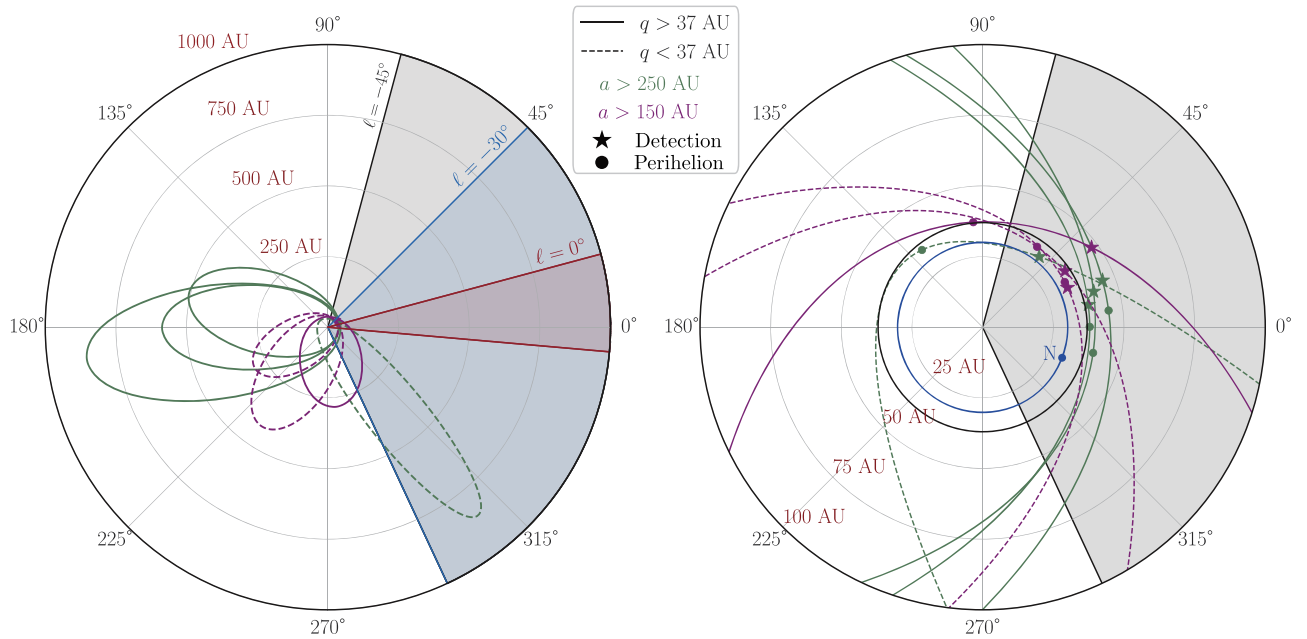
Figure 1. Ecliptic xy plane projection of the orbits of the seven eTNOs. The gray shaded sector in both panels represents the ecliptic extent of the DES footprint at ecliptic latitude $\ell = -45°$, and the longitudinal extent of the footprint at lower ℓ is denoted by the red ($\ell = 0°$) and blue ($\ell = -30°$) radial lines/sectors in the left panel. Solid lines represent orbits with $q > 37$ au, while dashed represent $30 < q < 37$ au. The green lines correspond to objects with $a > 250$ au, and the purple lines to the ones with $150 < a < 250$ au. The right panel presents a closer view of the orbits, with a star denoting the location of each object at the time of its detection and circles marking their perihelia. The blue circle marks Neptune's orbit (and the blue dot its location at barycentric Julian date 2016.0), and the black one represents a distance of 37 au from the center.

values of the ensembles remain very sensitive to small changes in the eTNO definition due to the small number of detections, which counsels further caution in assigning significance to the appearance of $p \approx 0.025$ values in our ensemble of tests. For example, adopting an eTNO definition of $a > 230$ au (following Brown 2017; Brown & Batygin 2019) yields p-values for the $\{\omega, \Omega, \varpi\}$ distributions of $\{0.468, 0.006, 0.532\}$, respectively. While the nodal clustering becomes apparently stronger, this is not the only variable in which Brown & Batygin (2019) find a signal for their sample, and there is no evidence for clustering in ω or ϖ, the variables in which they reported the strongest TNO alignments. Perhaps the most conservative approach would be to examine only the test for ϖ, which is the variable previously found to have the strongest clustering, using Case (4), which isolates the objects most sensitive to the dynamical effect of Planet 9 and least influenced by Neptune. For this single test, $p = 0.11$, meaning the null hypothesis of isotropy is rejectable with only 89% confidence.

One other statistic that we can use to judge the agreement between the observed and isotropized populations is the overall likelihood of the observed values of orbital angle $\theta \in \{\Omega, \omega, \varpi\}$:

$$\mathcal{L} \equiv p(\{\theta_j\}) = \prod_j p(\theta_j|s), \qquad (3)$$

taking the probability densities $p(\theta|s)$ directly from the simulation-derived histograms in Figure 2. While the ensemble likelihoods $\mathcal{L}$ are not themselves readily interpretable, we can produce an expected cumulative distribution function for $\mathcal{L}$ under the null hypothesis (isotropy) by calculating it for a large number of sets of "detections" drawn at random from the simulated population. We denote by f the fraction of sets of simulated isotropic detections that yield $\mathcal{L}$ lower than that for

the true detected objects. The f-test is more sensitive to individual objects being detected at the tails of the isotropic distribution, but unlike the Kuiper test, it does not consider the collective distribution. For example, the f-test would not register an abnormality if all the detections were on one side of a symmetric distribution. So the tests can be seen as complimentary and should not be expected to yield similar significance.

The f-values for each combination of orbital angle $\theta \in \{\Omega, \omega, \varpi\}$ and the eTNO definition are also listed in Table 2. For ϖ, all f-values are in the 20%–30% range and in the 50%–60% range for Ω, so the measured angles are not particularly likely or unlikely given the survey's selection functions. All eTNO definitions present a somewhat high f ($>90\%$) for ω, meaning that these detections are among the most likely outcomes possible given the isotropized distribution. This is not a surprise, since visual inspection of the ω selection functions (Figure 2) shows that all objects are in the region of highest probability. In sum, the $\mathcal{L}$ statistics are fully compatible with the null hypothesis of isotropy.

5. Alternative Analysis

A distinct analysis of the isotropy of DES eTNO detections is reported in full by Hamilton (2019), reaching the same conclusions as presented above, namely that the DES data do not by themselves offer strong evidence of alignments in the outermost known solar system. We highlight the major ways in which the Hamilton (2019) analysis differs from that presented above; details can be found in that publication.

1. Single-night transients were discovered using difference imaging (Kessler et al. 2015; Herner et al. 2020) rather than the catalog-level comparisons of Bernardinelli et al. (2020).
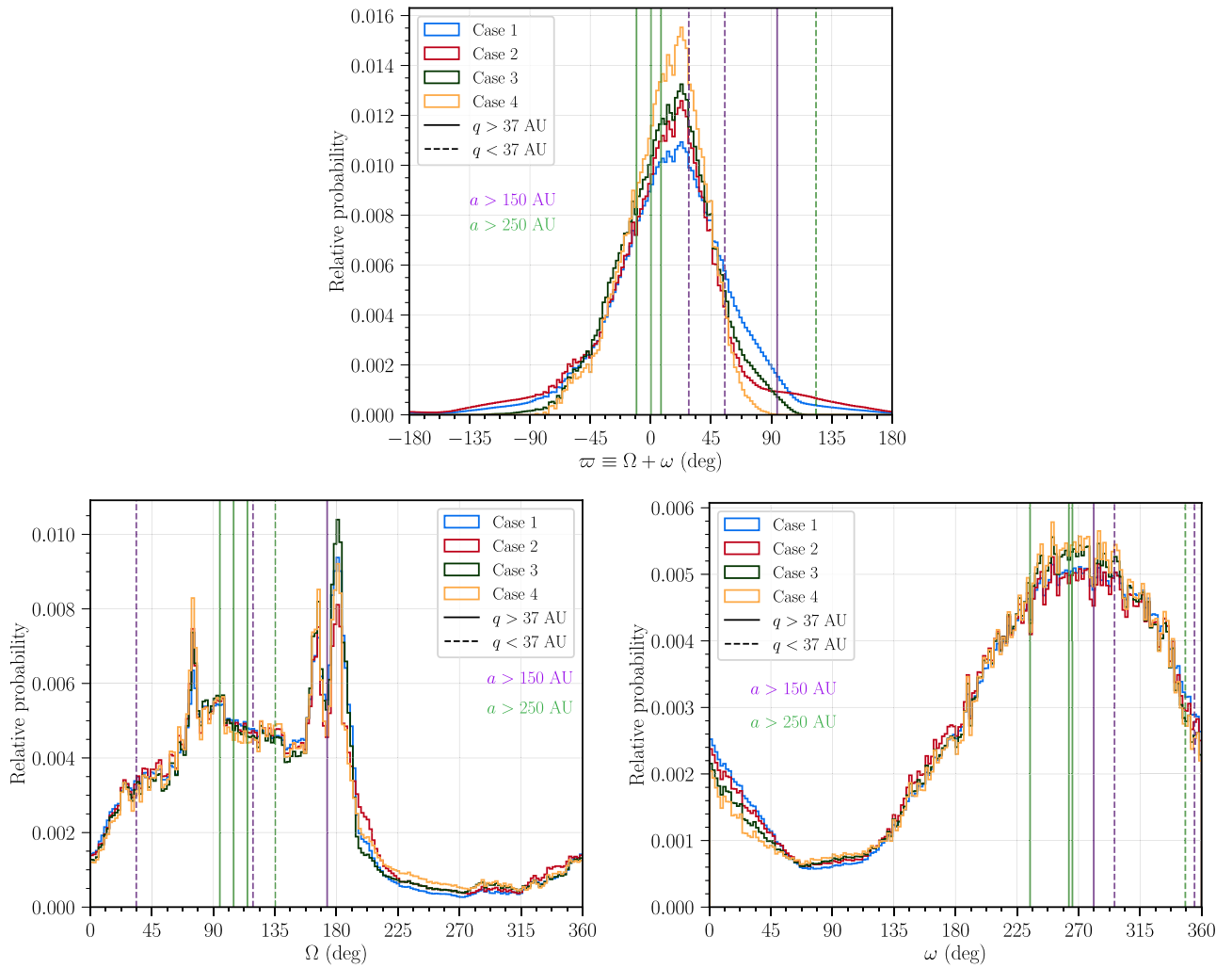
Figure 2. Relative probability histograms of Ω, ω, and ϖ for the *detected* members of a parent population constructed to be intrinsically isotropic in these variables while exactly reproducing the observed (a, e, i, and H) distribution of the detected objects. Histograms normalized to a common integral are shown for each of the four cases of eTNO definitions given in Section 2. Note that the angular selection functions are very robust regarding the definition of the underlying population. The vertical lines denote the angles at which objects were actually detected in the DES Y4 search. The line color denotes the semimajor axis range (purple, $150 < a < 250$ au and green, $a > 250$ au), and the line style denotes the perihelion range (dashed, $30 < q < 37$ au and solid, $q > 37$ au).

Table 2
p-values Derived Using Kuiper's Test Applied to the Four Distinct eTNO Definitions (Section 2) Studied here Measuring How Likely It Is that the Real eTNOs Come from a Uniform Underlying Distribution

Case	$p(\varpi)$	$f(\varpi)$	$p(\Omega)$	$f(\Omega)$	$p(\omega)$	$f(\omega)$
Case 1	0.933	0.235	0.180	0.595	0.393	0.960
Case 2	0.313	0.282	0.028	0.525	0.326	0.938
Case 3	0.361	0.192	0.211	0.628	0.053	0.973
Case 4	0.109	0.300	0.024	0.498	0.072	0.933

Note. The f-values represent the fraction of simulated isotropic detections that yield a likelihood $\mathcal{L}$ lower than the one for the true objects. Lower f- or p-values represent more significant deviations from isotropy.

2. The difference imaging was executed on a subset of the first three years of DES imaging rather than on the full Y4 data reported herein.
3. The alternative analysis includes TNOs discovered in the DES supernova search fields, whereas the Y4 analysis herein does not.
4. Different software and algorithms were used to link TNOs from the collection of detected transients.

5. The detection completeness of individual exposures for point sources was determined by measuring the signal-to-noise ratio (S/N) of sources of fixed, bright magnitude injected directly into the images and by calibrating this S/N level into a point-source completeness threshold (Kessler et al. 2015). The method of Bernardinelli et al. (2020) is to determine detection efficiency versus magnitude using faint stars in the fields.
6. The alternative analysis creates expected distributions for Ω, ϖ, and ω using a null hypothesis positing a chosen smooth distribution of sources in the space of $\{a, e, i, H\}$ with isotropy in $\{\Omega, \omega\}$, as opposed to this paper's technique of building the null-hypothesis population from isotropized copies of the discovered objects.

This difference-imaging search yields a sample of four TNOs meeting a definition of "extreme" as $a > 250$ au and $q > 30$ au, which is the same as case (2) above, although these are not the same four objects as in the case (2) analysis: 2013 RF$_{98}$ was discovered in the DES supernova search fields, while 2014 WB$_{556}$ had not been discovered.

Figure 5.1 of Hamilton (2019) present the null-hypothesis and the observed distributions of Ω, ω, and ϖ in analogy with Figure 2 above and looks very similar despite very different implementations of the processing steps. The Kuiper test statistic for departures from isotropy in Ω, ω, and ϖ are found to be exceeded by 8%, 24%, and 43% of the null-hypothesis distributions, respectively (see Figure 5.3). This leads to the same conclusions as the corresponding values of 3%, 32%, and 33% for Case 2 in Table 2.

6. Conclusion

We succeeded with little difficulty in creating an isotropic population model for eTNOs that matches the DES observations. The populations at $a > 250$ au are only marginally compatible with isotropy in Ω ($p \approx 0.025$ and $f \approx 0.5$), but this discrepancy is not strong enough to falsify the isotropy hypothesis given the small samples and multiple variables that we test. Similar to Shankman et al. (2017)'s analysis of the well-characterized OSSOS data, our analysis of the DES data does not present evidence of the Planet 9 hypothesis. We note that the consistency with an isotropic model does not falsify the Planet 9 hypothesis. Falsification would require that one show that *all* population models under this hypothesis are *inconsistent* with the data. The DES selection function is narrow in ϖ, reducing our sensitivity to true anisotropies. On the other hand, with a larger sample any ϖ distribution that is not constant across our limited window would eventually be detectable. When the full six years of DES observations are analyzed, the geometry of the selection functions should not change much, but the final catalog is expected to yield detections 0.5 mag deeper, likely increasing the total number of eTNOs in our sample.

ORCID iDs

Pedro H. Bernardinelli ⓘ https://orcid.org/0000-0003-0743-9422
Gary M. Bernstein ⓘ https://orcid.org/0000-0002-8613-8259
Masao Sako ⓘ https://orcid.org/0000-0003-2764-7093
Stephanie Hamilton ⓘ https://orcid.org/0000-0002-6126-8487
David W. Gerdes ⓘ https://orcid.org/0000-0001-6942-2736
Fred C. Adams ⓘ https://orcid.org/0000-0002-8167-1767
William R. Saunders ⓘ https://orcid.org/0000-0002-8737-742X
E. Gaztanaga ⓘ https://orcid.org/0000-0001-9632-0815
R. A. Gruendl ⓘ https://orcid.org/0000-0002-4588-6517
A. Palmese ⓘ https://orcid.org/0000-0002-6011-0530
A. R. Walker ⓘ https://orcid.org/0000-0002-7123-8943

References

Bailey, E., Batygin, K., & Brown, M. E. 2016, AJ, 152, 126
Bannister, M. T., Gladman, B. J., Kavelaars, J. J., et al. 2018, ApJS, 236, 18
Bannister, M. T., Kavelaars, J. J., Petit, J.-M., et al. 2016, AJ, 152, 70
Batygin, K., Adams, F. C., Brown, M. E., & Becker, J. C. 2019, PhR, 805, 1
Batygin, K., & Brown, M. E. 2016a, AJ, 151, 22
Batygin, K., & Brown, M. E. 2016b, ApJL, 833, L3
Batygin, K., & Morbidelli, A. 2017, AJ, 154, 229
Becker, J. C., Khain, T., Hamilton, S. J., et al. 2018, AJ, 156, 81
Bernardinelli, P. H., Bernstein, G. M., Sako, M., et al. 2020, ApJS, 247, 32
Brown, M. E. 2017, AJ, 154, 65
Brown, M. E., & Batygin, K. 2019, AJ, 157, 62
Flaugher, B., Diehl, H. T., Honscheid, K., et al. 2015, AJ, 150, 150
Gomes, R., Deienno, R., & Morbidelli, A. 2017, AJ, 153, 27
Hamilton, S. J. 2019, PhD thesis, Univ. Michigan http://hdl.handle.net/2027.42/151573
Herner, K., Annis, J., Brout, D., et al. 2020, arXiv:2001.06551

Kavelaars, J., Lawler, S. M., Bannister, M. T., & Shankman, C. 2020, in The Trans-Neptunian Solar System, ed. D. Prialnik, M. A. Barucci, & L. Young (Amsterdam: Elsevier), 61
Kessler, R., Marriner, J., Childress, M., et al. 2015, AJ, 150, 172
Khain, T., Becker, J. C., Adams, F. C., et al. 2018, AJ, 156, 273
Khain, T., Becker, J. C., Wen Lin, H., et al. 2020, AJ, 159, 133
Kuiper, N. H. 1960, Nederl. Akad. Wetensch. Proc. Ser. A, 63, 38
Lai, D. 2016, AJ, 152, 215
Lawler, S. M., Shankman, C., Kaib, N., et al. 2017, AJ, 153, 33
Lykawka, P. S., & Mukai, T. 2007, Icar, 189, 213
Madigan, A.-M., & McCourt, M. 2016, MNRAS, 457, L89
Shankman, C., Kavelaars, J. J., Bannister, M. T., et al. 2017, AJ, 154, 50
Sheppard, S. S., & Trujillo, C. 2016, AJ, 152, 221
Sheppard, S. S., Trujillo, C. A., Tholen, D. J., & Kaib, N. 2019, AJ, 157, 139
Trujillo, C. A. 2020, The Trans-Neptunian Solar System (Amsterdam: Elsevier), 79
Trujillo, C. A., & Sheppard, S. S. 2014, Natur, 507, 471
Zderic, A., Collier, A., Tiongco, M., & Madigan, A.-M. 2020, ApJ, 895, 27